

# ZnO based heterojunctions and nanostructures: Electrical transport mechanism and superior photocatalytic properties

M. Dutta and D. Basak

Department of Solid State Physics, Indian Association for the Cultivation of Science,  
Jadavpur, Kolkata 700032, India  
Email: sspdb@iacs.res.in

## Abstract

As the title suggests, the paper is presented with a two-fold objective- realization of stable p-type film and assembly of nanostructures keeping in mind the applications of ZnO in optoelectronics and water detoxification. Low-cost p-n heterojunction has been fabricated successfully by using the relatively stable sol-gel Al-N co-doped p-ZnO films on n-Si. The junction shows good diode characteristics with a rectification ratio  $\sim 10$  at 4 V in dark. Secondly, beaded nano-chains of ZnO have been synthesized by a novel technique using aqueous chemical method, which show superior photocatalytic property in the degradation of methyl orange in presence of ultraviolet radiation.

## 1. Introduction

ZnO is a promising short-wavelength optoelectronic material because of its direct wide band gap (3.437 eV at 2 K), large exciton binding energy ( $\sim 60$  meV) and high transparency ( $>80\%$ ) in the visible wavelength region [1]. ZnO also has other advantages such as non-toxicity, high quantum efficiency, greater resistance to high energy radiation, and the possibility of wet chemical etching. Two aspects of ZnO are still being focused as intensive research areas dealing with the issues of p-type conductivity and assembly of nanocrystallites.

Usually as-grown undoped ZnO films are n-type irrespective of the growth techniques. However, p-ZnO films are difficult to achieve due to the problems of low solubility of the acceptor dopants, self-compensation effects from the native donor defects ( $V_O$  and  $Zn_i$ ), deep acceptor levels, a hydrogen-like extrinsic donor etc [2, 3]. Despite of a substantial progress in the p-type films, the problems of stability, reproducibility and low hole concentration of the thin films remains. Among group V elements, N is predicted to be the most promising dopant

to realize p-type ZnO though the triumph of this dopant still lacks reproducibility [4, 5]. Yamamoto and Katayama-Yoshida [6] have proposed that the co-doping method with acceptors and reactive donors (Ga, In, Al etc.) may stabilize  $N_O$  substitution, which had been demonstrated to enhance N solubility. According to the theoretical predictions, Al-N co-doping has been found to be more effective than doping with Ga-N, since the corresponding III-N and III-O bonds are stronger for Al. Therefore, the prospects of Al-N co-doped ZnO films for the fabrication of p-n type of heterojunction using a chemical route appears to be unexplored till date.

Nanostructured ZnO has potential uses in efficient UV photodetection, UV lasing, energy conversion, gas sensing and catalysis [7, 8]. Now-a-days, ordered assembly of ZnO nanostructures for new applications are at the forefront of nanoscience and nanotechnology research. Different techniques of using templates, self-assembly nanosphere lithography, soft-lithography and self-seeded layers have been reported [8, 9]. However, removing the templates or the seed layers often become an issue in such

techniques. The polymer templates though can be removed easily, the assembly of the nanostructures is likely to be influenced by the surface interaction between polymer and ZnO. Therefore, an easier but cheaper technique for the assembly of free-standing ZnO nanostructures still remains to be a subject of research.

Keeping the above-mentioned issues in mind, the work reported in this paper is carried out based on two-fold objective. With the objective of realizing p-ZnO film using a low-cost sol-gel technique, p-ZnO (with Al-N co-doped)/n-Si heterojunction has been fabricated and its detailed transport mechanism has been predicted. Focusing on the other objective of attaining an ordered assembly of ZnO-based nanostructures, we report herein a very simple but novel technique to grow a beaded nanochain-like morphology by an aqueous chemical growth (ACG) method using Whatman (40) filter paper as the template. The synthesized nanostructures show enhanced photocatalytic activity for the degradation of methyl orange (MO) under UV irradiation. Depending on the objective, the paper content is divided into two sections, A and B where section A deals with the reports on p-type thin films and section B deals with the reports on assembly of ZnO nanostructures and their performance as photocatalyst.

## 2. Experimental details

A) p-type ZnO films and fabrication of heterojunction: The details of the deposition method is described elsewhere [10, 11]. In brief, to prepare N doped and Al-N co-doped p-ZnO films, a 0.4 M sol of zinc acetate 2-hydrate  $[Zn(CH_3COO)_2 \cdot 2H_2O]$  in isopropyl alcohol was prepared and stabilized by diethanolamine. Ammonium acetate  $[CH_3COONH_4]$  and aluminium nitrate  $[Al(NO_3)_3 \cdot 9H_2O]$  as nitrogen and aluminium sources, were added to the sol in the atomic ratio of Zn/N/Al of 1:1:0.01 and 1:1:0.02. The sol was spin coated on the cleaned n-Si (100) and glass substrates and dried at 120 °C in air followed by heating at 550 °C in oxygen. This process was repeated several times to obtain a film thickness of 550 nm measured by an ellipsometer (HORIBA Jobin Yvon, model HR460 FUV AGAS).

B) Assembly of ZnO nanostructures: An equimolar solution of (10mM)  $Zn(CH_3COO)_2$  and hexamethylenetetramine  $(CH_2)_6N_4$  in de-ionized water was prepared and taken in a glass beaker in which the filter

paper (Whatman 40) was held at 90 °C temperature for 30 min. The filter paper was then removed from the solution, rinsed with de-ionized water and dried followed by a calcination step at 700 °C in air to remove the paper [8].

The crystalline phase of ZnO was checked by an x-ray diffractometer (Seifert model XDAL 3000) using  $K_{\alpha}$  radiation. The electrical properties of the films were checked by using a Hall measurement system (ECOPIA model HMS-3000) in a Van der Pauw configuration. A field-emission scanning electron microscope (FESEM) (JEOL JSM-6700F) and a high-resolution transmission electron microscope (HRTEM) [JEOL JSM-2010] were used to study the morphology of the ZnO films and nanostructures.

## 3. Results and discussion

**Section A:** The X-ray diffractograms of the undoped and doped ZnO films are shown in Fig. 1. The diffraction peaks of all the films are identified as (100), (002), (101), (102), (110), (103) and (112) plane of reflections of a wurtzite structure of ZnO. The FESEM images of the films in

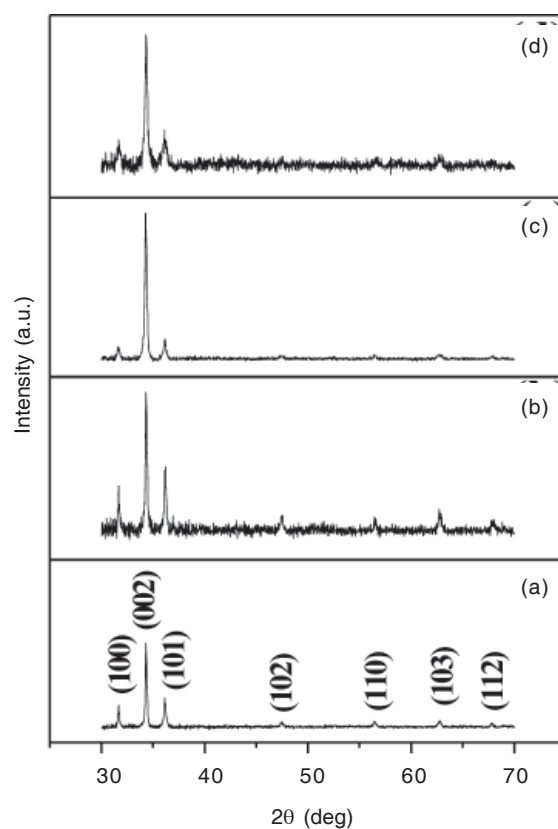


**Fig. 1.** X-ray diffractograms of the films (a) ZnO, (b) ZnO:N (1:1) (c) ZnO:N:Al (Zn/ N/Al = 1:1:0.01), (d) ZnO:N:Al (Zn/ N/Al = 1:1:0.02).

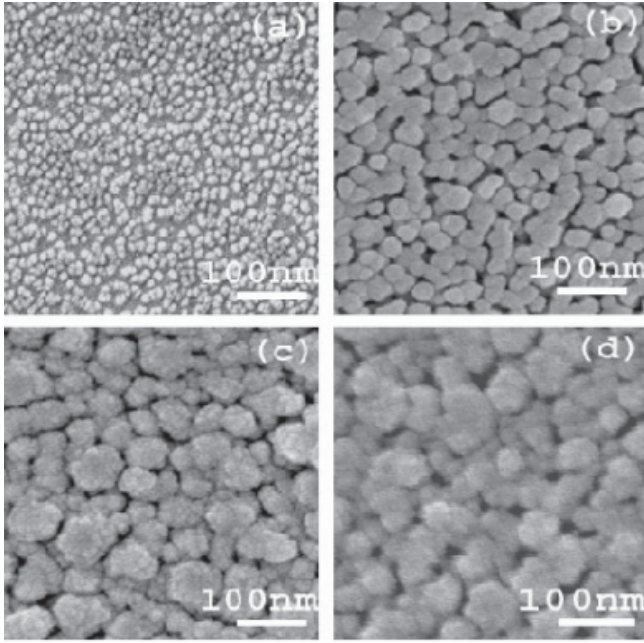


**Fig. 2.** FESEM images of the films (a) ZnO, (b) ZnO:N (1:1) (c) ZnO:N:Al (Zn/ N/Al = 1:1:0.01), (d) ZnO:N:Al (Zn/ N/Al = 1:1:0.02).

Figure 2 shows that all the films consist of grains where the grain size increases from 17 - 25 nm for the undoped ZnO to 50-60 nm for the N-doped and to 70-76 nm for the Al-N co-doped films.

The Hall measurement data for all the films are shown in Table 1. The difference in the carrier concentration values when the films are prepared in air and oxygen ambient (Table 1) clearly indicates that the number of background carrier concentration is suppressed leading to an insulating film. The N-doped film shows an unstable behavior. The carrier type is found to be fluctuating between p-type and n-type. The Al-N co-doped film shows relatively a stable p-type conductivity (Table 1). This indicates that the co-doping technique may be an effective way to incorporate

**Table 1.** The values of the hole or electron concentration, mobility and resistivity of the ZnO thin films. All the films except the air annealed one are annealed in oxygen ambient.

Sample	Concentration (cm <sup>-3</sup> )	Mobility (cm <sup>2</sup> /Vs)	Resistivity (Ω-cm)
Undoped	(-) $8.5 \times 10^{12}$	53.5	13743
Undoped (Air annealed)	(-) $5 \times 10^{17}$	0.32	39
N-doped (Zn/N=1:1)	(-) $6.53 \times 10^{13}$ – (+) $5.95 \times 10^{14}$	66.5– 6.4	1440– 1643
Al-N codoped (Zn/N/Al=1:1:0.01)	(+) $2 \times 10^{17}$	1.6	19
Al-N codoped (Zn/N/Al=1:1:0.02)	(+) $8 \times 10^{16}$	1.73	45

N. Doping with only N causes a strong repulsive potential, thereby creating a large distance (6.14 Å) between the two N atoms which causes the low solubility and instability of N in the p-type film. However, there is also a possibility of nonuniform distribution of N in the film without Al. The Al-N co-doping reduces the repulsive potential between N atoms which reduces the distance to 4.57 Å thus increasing the incorporation of N [6]. The Al-N co-doped film (Zn/N/Al = 1:1:0.01) has been employed to form heterojunction with n-Si (resistivity and carrier concentration 4-6 Ω-cm and  $1 \times 10^{15}$  cm<sup>-3</sup> respectively). The I-V characteristic of the heterojunction in figure 3(a) exhibits a good rectifying behavior with a  $I_F/I_R \sim 10$  at 4 V indicating formation of a diode ( $I_F$  and  $I_R$  stand for the forward and reverse current respectively). Though the rectification ratio is smaller than the value ( $\sim 24$  at  $\sim 4$  V) for the molecular beam epitaxy (MBE) grown p-ZnO-based heterojunction observed by Mandalapu et al.[13], is better than that ( $\sim 6$  at  $\sim 4$  V) observed by Zhuge et al. [14] for the sputtered junction. The turn-on-voltage and reverse leakage current values are found to be 1.16 V and  $5.517 \times 10^{-7}$  A at  $-4$  V (equivalent to  $6.1 \times 10^{-5}$  A/cm<sup>2</sup> taking into account the contact area) respectively in dark. Before explaining the transport mechanism, it is necessary to understand the energy band diagram of the junction based on Anderson's model [15] given in Fig. 3(b). The band gap and electron affinity values for ZnO and Si are  $E_{g, ZnO} = 3.36$  eV (Fig. 2(c)),  $\chi_{ZnO} = 4.35$  eV and  $\chi_{Si} = 4.05$  eV,  $E_{g, Si} = 1.12$  eV respectively [10]. The model shows a small conduction band offset (0.3 eV) and a large valence band offset (2.54 eV). All the log-log plots of I vs V (figure 4) show three regions. In the dark, for a very low bias voltage i.e  $< 1.6$  V (region I), the diode shows a high resistance probably due to the presence of a thin SiO<sub>2</sub> layer limiting the current and hence the dark current increases linearly in this region (figure 4). For  $1.6 < V < 3.3$  V (region II), the current increases exponentially following the equation  $I \sim \exp(\alpha V)$ , which is usually observed in the wide band gap p-n diodes due to recombination-tunneling mechanism [16, 17]. The constant  $\alpha$  has been evaluated to be  $1.45$  V<sup>-1</sup> by fitting the experimental data in figure 4 which falls in the range of 0.45 to  $1.50$  V<sup>-1</sup> for the semiconductor junctions as

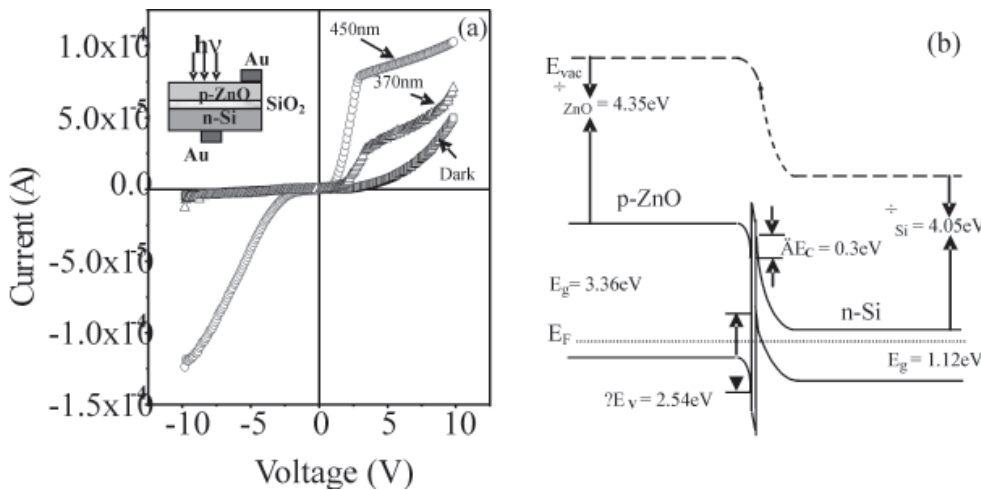


**Fig. 3.** (a) I-V Characteristics of the p-ZnO/n-Si heterojunction. The insets show the schematic diagram of the p-ZnO/n-Si heterostructure. (b) The energy Band diagram of the junction at zero bias.

suggested by Fedison et al.[16] When  $V > 3.6$  V (region III), the I-V characteristic follows a power law  $I \sim V^2$  (the inset of figure 4) where the current conduction is attributed to the space-charge limited current (SCLC) for a single carrier (hole) injection since concentration of the holes are larger than the electrons in the present case. This SCLC mechanism is a normal phenomenon in the wide band gap semiconductors [17]. Our p-ZnO film is highly transparent to the visible light [11] and absorbs UV light meaning that e-h pairs are produced in the layer when it absorbs UV photons. These photo-generated holes take part in the conduction process increasing the current exponentially. The current for UV light in figure 4 initially increases linearly with bias voltage below 0.67 V (region I) and then follows

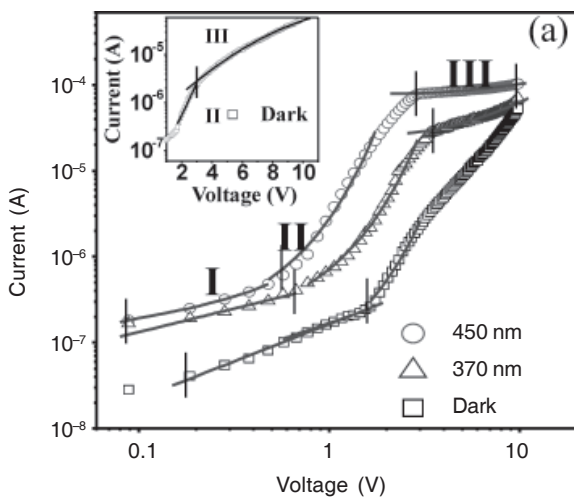


**Fig. 4.** Log-log plots of the injection current vs voltage in forward bias and inset shows the semi log plot of dark current vs voltage in forward bias.

the equation  $I \sim \exp(\alpha V)$  for  $0.76 < V < 3$  (region II). By exponential fitting of the experimental data, the value of  $\alpha$  has been evaluated to be  $1.7 \text{ V}^{-1}$  which explains the high carrier injection. Beyond 3.5 V (region III), the experimental curve could be fitted perfectly with a power equation with an exponent of 2 suggesting SCLC mechanism. Under the reverse bias conditions, as the depletion width increases, the photo-generated carriers

are trapped in ZnO resulting no increase in the net current. When visible light (450 nm) falls on the junction, it passes through the ZnO layer and absorbed in the underlying n-Si, generating e-h pairs, and these photo-generated electrons are easily drifted towards p-ZnO side owing to the small conduction band offset value contributing to the current conduction. Thus, initially, after a linear increase in the current below 0.47 V (region I), the current increases exponentially following the equation  $I \sim \exp(\alpha V)$  (region II) up to 1.74 V (figure 4). The evaluated  $\alpha$  value of  $3.2 \text{ V}^{-1}$  suggests the high carrier (electrons) injection. Beyond 3 V (region III), the power law dependence of the I-V curve suggests the SCLC. The increase of reverse current with 450 nm is probably due to drifting of holes towards p-ZnO side [13].

**Section B:** For assembly, Whatman filter paper was coated with ZnO (figures 5(a)) which shows that the nanoparticles align themselves along the axis of the fibrils in a highly organized fashion indicating that the fibers act as the nucleating substrates. The TEM images in figure 5 (b) and (c) show microstructures of the template-grown ZnO. The crystallites are joined as beads to form a nanochain-like morphology. The average diameter of the beads is in the range 34 nm to 54 nm. The decomposition efficiency of MO can be calculated using the following expression:

$$\text{MO decomposition (\%)} = (C_0 - C) / C_0 \times 100 \quad (1)$$

where  $C_0$  and  $C$  are the equilibrium concentration of MO before and after the UV irradiation, respectively. Figure 7

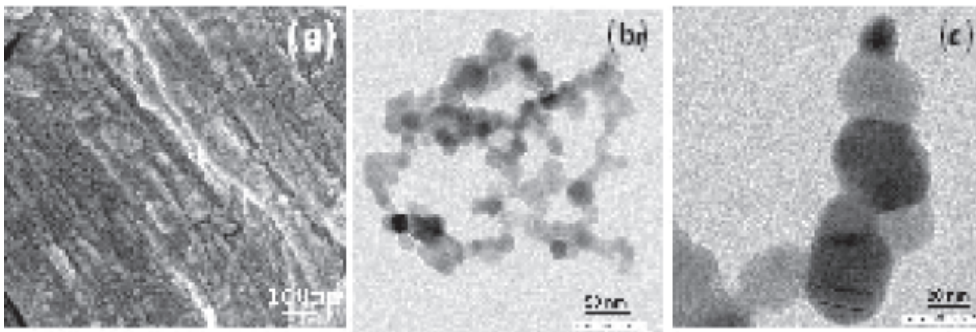


**Fig. 5.** (a) FESEM image of template grown ZnO nanostructure, (b) and (c) TEM images of the template-grown, calcined ZnO nanostructures

shows the kinetics of MO photodegradation without and with the presence of both beaded and lumped ZnO nanostructures. While MO is degraded negligibly without the presence of ZnO, about 64% and 22% degradation is occurred after the UV irradiation for 2 h 45 min in case of the beaded and the lumped nanostructure respectively. The superior photocatalytic property of the template grown sample is responsible for the higher surface area of the interconnected nanostructure which produces a fast electron transfer process making the photocatalytic reaction faster.

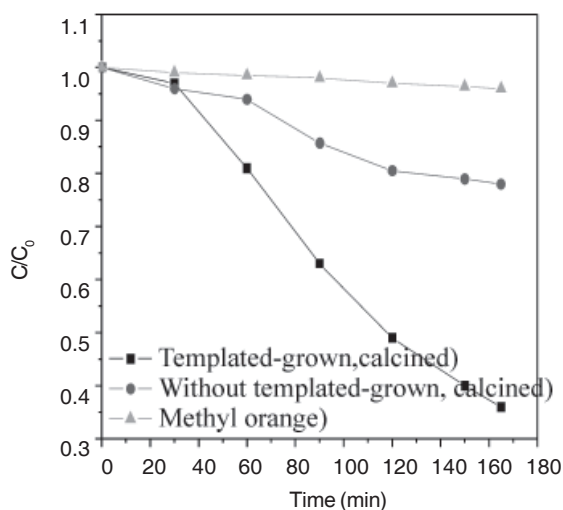


**Fig. 6.** Photodegradation kinetics of MO in the presence of ZnO nanostructures.



**Mrinal Dutta** completed his Bachelor's and Masters degree in Physics from the University of Burdwan in the years 2003 and 2005 respectively. He has already submitted his Ph. D. thesis to the Jadavpur University in 2010. His research interest involves structural, electrical and optical properties of wide band gap semiconducting thin films, quantum dots and synthesis of carbon nanotube based composite structures. He has to his credit nine published papers in international journals. Mrinal received the third best award for YPC 2010 jointly with Mr. Bhushan Joshi.

#### 4. Conclusion

The Al-N co-doped ZnO film forms good heterojunction with n-Si and its current transport mechanism has been explained. Beaded nano-chains grown by ACG method show superior photocatalytic activity in the degradation of MO.

#### References

1. D.C. Look, *Mater. Sci. Eng. B* **80**, 383 (2001).
2. C.H. Park, S.B. Zhang, and S.H. Wei, *Phys. Rev. B* **66**, 073202 (2002).
3. C.G. Van de Walle, *Phys. Rev. Lett.* **85**, 1012 (2000).
4. Y.W. Heo, Y.W. Kwon, Y. Li, S.J. Pearton, and D.P. Norton, *J. Electron. Mater.* **34**, 409 (2004).
5. Y.R. Ryu, S. Zhu, D.C. Look, J.M. Wrobel, H.M. Jeong, and H.W. White, *J. Cryst. Growth* **216**, 330 (2000).
6. T. Yamamoto and H. Katayama-Yoshida, *Jpn. J. Appl. Phys.* **38**, L166 (1999).
7. S. S. Hullavarad, N. V. Hullavarad, P. C. Karulkar, A. Luykx and P. Valdivia, *Nanoscale Res. Lett.* **2**, 161 (2007).
8. M. Dutta and D. Basak, *Nanotechnology*, **20**, 475602 (2009).
9. R. Ghosh, M. Dutta and D. Basak, *Appl. Phys. Lett.* **91**, 073108 (2007).
10. M. Dutta and D. Basak *Appl. Phys. Lett.* **92**, 212112 (2008).
11. M. Dutta, T. Ghosh and D. Basak, *J. Electron. Mater.* **38**, 2335 (2009).
12. M. Dutta and D. Basak, *Chem. Phys. Lett.* **480**, 253 (2009).
13. L. J. Mandalapu, F. X. Xiu, Z. Yang, D. T. Zhao, and J. L. Liu, *Appl. Phys. Lett.* **88**, 112108 (2006).
14. F. Zhuge, L. P. Zhu, Z. Z. Ye, D. W. Ma, J. G. Lu, J. Y. Huang, F. Z. Wang, Z. G. Ji, and S. B. Zhang, *Appl. Phys. Lett.* **87**, 092103 (2005).
15. S. M. Sze, *Physics of Semiconductor Devices*, 2nd ed. (Wiley, New York, 1981).
16. J. B. Fedison, T. P. Chow, H. Lu, and I. B. Bhat, *Appl. Phys. Lett.* **72**, 2841 (1998).
17. R. Ghosh and D. Basak, *Appl. Phys. Lett.* **90**, 243106 (2007).